An Application of Fast Integral Wavelet Transform to Waveguide Mode Identification

Jaideva C. Goswami, *Student Member, IEEE,* Andrew K. Chan, *Senior Member, IEEE,* and Charles K. Chui, *Fellow, IEEE*

***Abstract*—We introduce a very efficient method for computing the integral wavelet transform, with any compactly supported spline-wavelet as the analyzing wavelet, on a dense set of the time-scale domain. While the mathematical analysis of this algorithm will be presented elsewhere, the objective of this paper is to describe the computational scheme along with its computer implementation, and to demonstrate its effectiveness in the identification of mode propagation in a rectangular waveguide.**

***Index Terms*—Wavelet transform, waveguide modes.**

I. Introduction

THE INTEGRAL wavelet transform (IWT) is a time-frequency localization tool with automatic "zoom-in" and "zoom-out" bandpass filter performance. However, since it is a mapping of functions (or analog signals) of one variable (the time domain) to functions of two variables (the time-scale domain), computation of the IWT in all of the time-scale domain is certainly very expensive. Although the wavelet decomposition algorithm, based on certain digital samples—say $f(k/2^N)$, $k = \cdots, -1, 0, 1, \cdots$ of some signal $f(t)$—can be applied with real time capability to give the IWT values of $f(t)$ at $(k/2^j, 1/2^j)$, $k = \cdots, -1, 0, 1, \cdots$, and $j \leq N - 1$, this information on the IWT of $f(t)$, on such a sparse set of dyadic points, is sometimes insufficient to give very good time-frequency analysis of the signal $f(t)$.

The objective of this paper is to describe a very efficient algorithm that we just developed [24] for computing the IWT of $f(t)$ on a dense set of the time-scale domain, without going into the somewhat complicated mathematical details. In addition, we include several examples to elucidate the application of this algorithm.

In applications to discrete data sets, wavelets may be considered as basis functions generated by dilations and translations of a single function. Analogous to Fourier analysis, there are wavelet series (WS) and integral wavelet transforms. However, unlike Fourier analysis, WS and IWT are intimately related in wavelet analysis. Fourier analysis is a global analysis in the sense that each frequency (time) component of the function is influenced by all the time (frequency) components of the function. On the other hand, wavelet analysis is a local analysis. Such comparisons are very well reported in [11]–[13].

Wavelets have drawn a lot of attention in recent years because of their versatility in many areas of engineering, physics, and mathematics. From the engineering point of view, there are broadly two different objectives of applying wavelet analysis. In one, the function (continuous or discrete) is known in some domain (time, for example) and one is interested in observing the behavior of the function in the time-frequency domain. In the other, the function is not known explicitly but some of its properties are known along with the function behavior on a certain known set of points. Here the objective is to specify the function. Significant work has been reported for the former case. As to the applications to electrical engineering, although wavelets have a great impact in the area of signal processing, the literature is scant on BVP. Work in integral equations has been reported in [1]–[5]. It has been demonstrated that the use of wavelet bases results in sparse matrix for integral operators. In [6]–[10], problems related to differential operator and bounded interval wavelets are discussed.

There have been a few papers related to wavelets in the area of Electromagnetics [13]–[17]. In [13], [18] it has been demonstrated that time-frequency analysis provides better information about the EM scattering phenomena. Steinberg and Leviatan [16] have used the Battle-Lemarié spline-wavelets as basis in the method of moments formulation. Although any Battle-Lemarié wavelet generates an orthogonal basis, it has poor decay at infinity and does not have closed form expression. On the other hand, compactly supported spline-wavelets [11], [19], which will be used in this paper are semi-orthogonal with explicit closed form expressions. Here, we will point out that the coefficients of the dual of these wavelets are infinite although they decay exponentially fast. It will be shown in this paper that by mapping the function into some proper subspace, one can circumvent the use of dual wavelets to compute the wavelet coefficients (WC). Multigrid FEM is another area in which wavelets are being applied. Multilevel discretization concept has been used in [20] in the context of method of moments.

In [13], a brief discussion on multiresolution analysis (MRA) has been presented, but it has not been used to compute the WC. Instead, FFT has been applied to compute the IWT with Kaiser-Bessel window as wavelet; the same window has been used in [18] to compute the short-time Fourier transform (STFT). In MRA-based computation of

Manuscript received September 9, 1993; revised May 27, 1994. This work was supported in part by the Texas Higher Education Coordinating Board under grant numbers 999903-049 and 999903-054 and ARO contract DAAH 04-93-G0047.

J. C. Goswami and A. K. Chan are with the Electromagnetics and Microwave Laboratory, Department of Electrical Engineering, Texas A&M University, College Station, TX 77843-3128 USA.

C. K. Chui is with the Center for Approximation Theory, Department of Mathematics, Texas A&M University, College Station, TX 77843-3368 USA.

IEEE Log Number 9407466.

the WC, the complexity, usually defined in terms of number of multiplications and additions per point, remain the same irrespective of the scale, which is not the case with FFT-based method. This aspect will be further elaborated in Sections III and IV.

The rest of this paper is organized as follows. Section II begins with a brief introduction of the notion of MRA. The integral wavelet transform and the standard wavelet decomposition algorithm are presented. A few important properties of splines and spline wavelets follow next. Wavelet transform gives local time-scale information. In order to translate this into time-frequency information, the scale parameter needs to be mapped into frequency. A method is proposed to obtain such mapping. In Section III, we present a technique to compute the WC with finer time-scale resolution. A few examples are discussed in Section IV that include the IWT of the experimental data obtained for the transmission coefficient of a rectangular waveguide. The results are obtained using linear and cubic splines and their corresponding compactly supported wavelets. With a little more work, the method can be extended to splines of arbitrary order.

II. MRA and Wavelet Decomposition

A. MRA and Wavelet Decomposition

As the name suggests, in MRA, a function is viewed at various levels of approximations or different resolutions. The idea was developed by Meyer [21] and Mallat [22]. Any cardinal B-spline generates an MRA. More precisely, consider the integer translates of a function $\phi \in L^2 := L^2(\mathbb{R})$ (finite energy function). This collection constitutes an approximation space V_0, where for each j, we use the notation

$$V_j := clos_{L^2}\langle \phi_{j,k} : k \in \mathbb{Z}\rangle, \quad j \in \mathbb{Z} \tag{1}$$

with $\phi_{j,k}(t) := 2^{j/2}\phi(2^j t - k)$ and $\mathbb{Z} := \{\cdots, -1, 0, 1, \cdots\}$. Here the function ϕ is a cardinal B-spline with integer knots of an appropriate order, or more generally, a scaling function. The subspaces $\{V_j\}$ are nested, namely

$$\cdots \subset V_{-1} \subset V_0 \subset V_1 \subset \cdots . \tag{2}$$

For a precise definition of MRA, see [11, p. 16].

For each j, since $V_j \subset V_{j+1}$, we have the orthogonal complementary wavelet subspace W_j such that

$$V_{j+1} = V_j \oplus W_j \tag{3}$$

where

$$W_j := clos_{L^2}\langle \psi_{j,k} : k \in \mathbb{Z}\rangle, \quad j \in \mathbb{Z} \tag{4}$$

and $\psi_{j,k}$ is defined similarly to $\phi_{j,k}$.

It is to be observed here that while $\{V_j\}$ form a nested sequence of subspaces, the subspaces $\{W_j\}$ are mutually orthogonal. Consequently,

$$\begin{aligned} V_j \cap V_\ell &= V_j \qquad \ell > j \\ W_j \cap W_\ell &= \{0\} \qquad j \neq \ell. \end{aligned} \tag{5}$$

At any level j, V_j gives the smoothing "approximation" and W_j reveals the "details" of the original function.

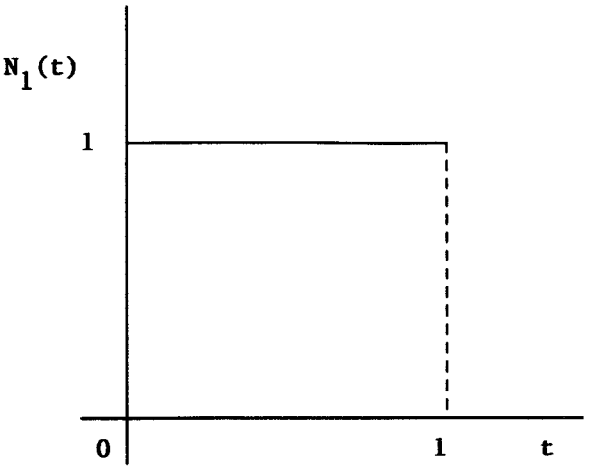

Fig. 1. N_1, the spline of order 1.

B. Splines and Spline Wavelets

In this paper, we use cardinal B-splines N_m to be the scaling functions. Here, for any positive integer m, called the order of the B-spline N_m, a fast computation of $N_m(t)$ can be achieved by using the following formula [11, p. 86] recursively until we arrive at

$$N_m(t) = \frac{t}{m-1}N_{m-1}(t) + \frac{m-t}{m-1}N_{m-1}(t-1) \tag{6}$$

the first-order B-spline N_1, which is simply the characteristic function $\chi_{[0,1)}$. (See Fig. 1.)

One of the most important properties of a B-spline is "total positivity" [23, p. 7], by virtue of which the function in terms of a B-spline series follows the shape of the "data." For instance, if $g(t) = \Sigma_j \alpha_j N_m(t-j)$, then

$$\begin{aligned} \alpha_j \geq 0 \,\forall j &\Rightarrow g(t) \geq 0 \\ \alpha_j \uparrow (\text{increasing}) &\Rightarrow g(t) \uparrow, \quad \text{and} \\ \alpha_j (\text{convex}) &\Rightarrow g(t) \,\text{convex}. \end{aligned} \tag{7}$$

Furthermore, the number of sign changes of $g(t)$ does not exceed that of the coefficient sequence $\{\alpha_j\}$.

Any function $f(t) \in L^2$ can be mapped into a spline space of order m as

$$f(t) \mapsto f_M(t) = \sum_k c_k^M \phi(2^M t - k) \in V_M, \tag{8}$$

where, as mentioned before, we will choose $\phi = N_m$. For $m = 1$, we have an orthonormal basis, but for $m > 1$, $\{N_m(t-k)\}$ is no longer orthonormal, but is a so-called Riesz or stable basis [11] of V_0. Hence, for $m > 1$, in order to get $\{c_k^M\}$, one needs to have the dual of ϕ, $\tilde{\phi}$. By duality, we mean

$$\langle \phi(\cdot - k), \tilde{\phi}(\cdot - \ell)\rangle = \delta_{k,\ell}, \quad \text{all } k, \ell, \tag{9}$$

where $\delta_{k,l}$ is the Kronecker delta

$$\delta_{k,\ell} = \begin{cases} 1 & \text{if } k = \ell \\ 0 & \text{otherwise.} \end{cases}$$

Orthonormal bases are self-dual. Using (8) and (9), we have

$$c_k^M = 2^M \int_{-\infty}^{\infty} f_M(t)\overline{\tilde{\phi}(2^M t - k)}\, dt. \tag{10}$$

Observe that 2^M appears in (10) because of the biorthogonality

property, namely

$$\langle \phi_{j,k}, \tilde{\phi}_{\ell,m} \rangle = \delta_{j,\ell}\delta_{k,m}. \tag{11}$$

Corresponding to each scaling function, we have a wavelet. By means of the so-called "two scale relations," one can construct a wavelet as follows:

$$\phi(t) = \sum_k p_k \phi(2t-k),$$
$$\psi(t) = \sum_k q_k \phi(2t-k). \tag{12}$$

For m^{th} order splines, we have [11], [19]:

$$p_k = \begin{cases} 2^{-m+1}\binom{m}{k} & 0 \le k \le m \\ 0 & \text{otherwise,} \end{cases}$$

and

$$q_k = (-1)^k 2^{-m+1} \sum_{\ell=0}^{m} \binom{m}{\ell} N_{2m}(k+1-\ell)$$
$$k = 0, 1, \cdots, 3m-2. \tag{13}$$

A function $f(t)$ can also be represented in terms of some wavelet ψ, namely

$$f(t) = \sum_{j,k} d_k^j \psi(2^j t - k), \tag{14}$$

where

$$d_k^j = 2^j \int_{-\infty}^{\infty} f(t)\overline{\tilde{\psi}(2^j t - k)}\, dx, \tag{15}$$

and $\tilde{\psi}$ is the dual of ψ defined in a similar way as $\tilde{\phi}$, the dual of ϕ. Unlike "total positivity" of splines, the wavelets have a so-called "complete oscillation" property by virtue of which the wavelet coefficients $\{2^{-j/2} d_k^j\}$ help in detecting any change in the function behavior. Note that $2^{-j/2}$ has been used as the multiplier so that WC represent IWT of the function at dyadic positions and binary scales. (See (23).)

One of the most important properties of the mth-order spline wavelet ψ_m is that their moments with respect to lower degree polynomials are zero. More precisely,

$$\int_{-\infty}^{\infty} t^p \psi_m(t)\, dt = 0, \qquad p = 0, 1, \cdots, m-1. \tag{16}$$

The importance of (16) will become more apparent in Section IV.

Fig. 2 shows the linear ($m = 2$) and cubic ($m = 4$) splines with their corresponding wavelets in the time domain. Their frequency-domain representations are shown in Fig. 3. It is obvious from Fig. 3 that scaling functions behave as lowpass filters, whereas wavelets exhibit bandpass filter characteristics.

Equations (10) and (15) indicate that the coefficients are obtained by convolving the function with scaling function and wavelet. This amounts to, from the filter-bank theory, passing the function (signal) through a lowpass filter for $\{c_k\}$ and a bandpass filter for $\{d_k\}$.

C. The Integral Wavelet Transform (IWT) and Wavelet Decomposition

The IWT of a function $f(t) \in L^2$ with respect to some analyzing wavelet $\tilde{\psi}$ is defined as

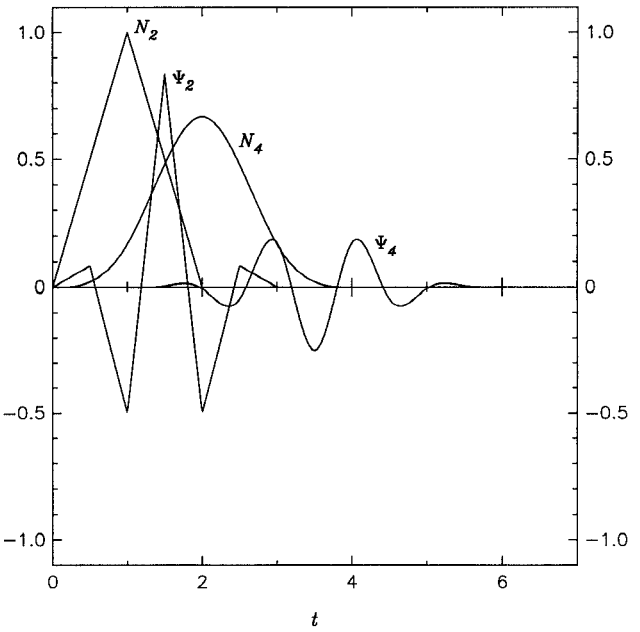

Fig. 2. Linear and cubic splines with corresponding wavelets in time domain.

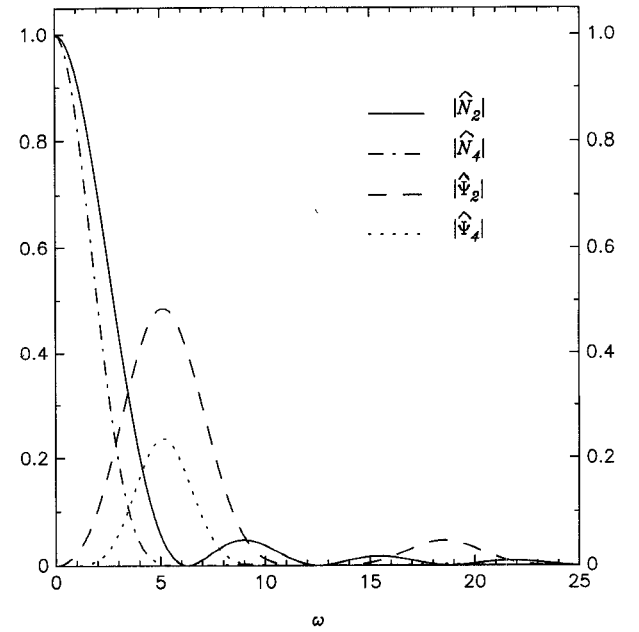

Fig. 3. Linear and cubic splines with corresponding wavelets in frequency domain indicating the low pass and band pass filter characteristics of scaling functions and wavelets, respectively.

$$(W_{\tilde{\psi}} f)(b,a) := \int_{-\infty}^{\infty} f(t)\overline{\tilde{\psi}_{ab}}(t)\, dt, \tag{17}$$

where

$$\tilde{\psi}_{ab}(t) = a^{-(1/2)}\tilde{\psi}\left(\frac{t-b}{a}\right), \tag{18}$$

and $a > 0$ is the dilation and b, the translation parameters. The normalization factor $a^{-(1/2)}$ is included so that $||\tilde{\psi}_{ab}|| = ||\tilde{\psi}||$ where $||\cdot||$ implies L^2 norm.

To recover $f(t)$ from (17), and for $\tilde{\psi}$ to be a window function, the zeroth moment of $\tilde{\psi}$ must vanish [11], namely

$$\int_{-\infty}^{\infty} \tilde{\psi}(t)\,dt = \hat{\tilde{\psi}}(0)\,dt = 0, \tag{19}$$

where $\hat{\tilde{\psi}}$ is the Fourier transform of $\tilde{\psi}$.

The wavelet $\tilde{\psi}$ is localized in both time as well as frequency. By reducing a, the support of ψ_{ab} reduces in time and hence covers a large frequency range and vice-versa. Therefore, $1/a$ is a measure of frequency. The parameter b, on the other hand, indicates the location of the wavelet window in time. Thus by changing (b, a), the whole time-scale plane can be covered.

The first step towards decomposing a function $f(t)$ is to map the given function (in the form of one-dimensional data) into a spline space, namely

$$f(t) \mapsto f_M(t) \in V_M. \tag{20}$$

The approximate function $f_M(t)$ can be decomposed as follows:

$$f_M(t) = g_{M-1}(t) + \cdots + g_{M-M'}(t) + f_{M-M'}(t) \tag{21}$$

where $M' < M$, and

$$\begin{aligned} V_j \ni f_j(t) &= \sum_k c_k^j \phi(2^j t - k) \\ W_j \ni g_j(t) &= \sum_k d_k^j \psi(2^j t - k). \end{aligned} \tag{22}$$

The function $g_j(t)$ gives the "details" at the level j, whereas $f_j(t)$ gives the approximation of the original function at the level j, which is coarser than that at the level $j+1$.

The importance of this decomposition algorithm is that we have

$$2^{-j/2} d_k^j = W_{\tilde{\psi}} f_M\left(\frac{k}{2^j}, \frac{1}{2^j}\right) \tag{23}$$

and, for any $j < M$,

$$(W_{\tilde{\psi}} g_j)\left(\frac{k}{2^j}, \frac{1}{2^j}\right) = (W_{\tilde{\psi}} f_M)\left(\frac{k}{2^j}, \frac{1}{2^j}\right), \tag{24}$$

for all integers k.

From the highest level approximation coefficient sequence $\{c_k^M\}$, we can get the lower level sequences $\{c_k^j\}$ and $\{d_k^j\}$ as follows:

$$\begin{aligned} c_k^j &= \sum_\ell a_{2k-\ell} c_\ell^{j+1} \\ d_k^j &= \sum_\ell b_{2k-\ell} c_\ell^{j+1}, \end{aligned} \tag{25}$$

where $\{a_k\}$ and $\{b_k\}$ are known once the B-spline and the B-wavelet are fixed.

D. Scale-to-Frequency Mapping

The integral wavelet transform of a function gives its local time-scale information. In order to get the time-frequency information, we need to map the scale parameter to frequency. There is no general way of doing so. However, as a first approximation, we may consider the following mapping:

$$a \mapsto f := \frac{c}{a} \tag{26}$$

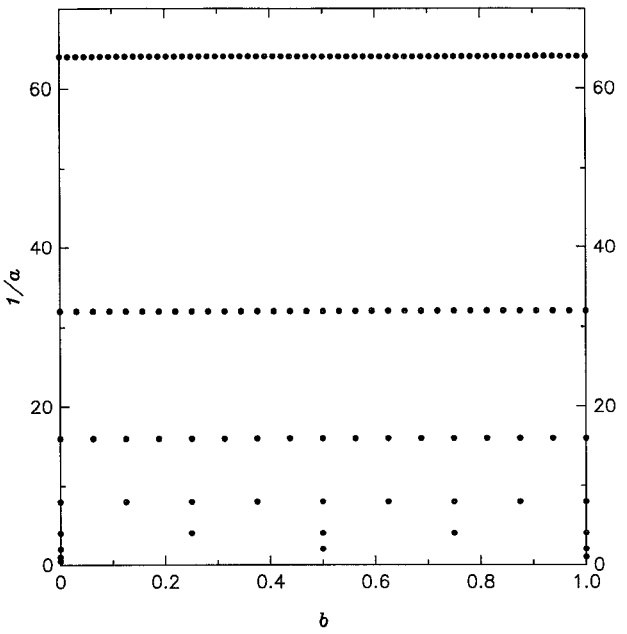

Fig. 4. A typical time-scale grid from the standard wavelet decomposition algorithm applied to a function with support [0, 1] and discretization step as 0.25. Only points in [0, 1] are shown.

where $c > 0$ is a calibration constant. In this paper the constant c has been determined based on the one-sided center (ω_+^*) and one-sided radius $(\Delta\hat{\psi}_+)$ of the wavelet $\hat{\psi}(\omega)$, which are defined as in [27]:

$$\omega_+^* := \frac{\int_0^\infty \omega |\hat{\psi}(\omega)|^2\,d\omega}{\int_0^\infty |\hat{\psi}(\omega)|^2\,d\omega} \tag{27}$$

$$\Delta\hat{\psi}_+ := \frac{\int_0^\infty (\omega - \omega_+^*)^2 |\hat{\psi}(\omega)|^2\,d\omega}{\int_0^\infty |\hat{\psi}(\omega)|^2\,d\omega}. \tag{28}$$

For cubic spline we get $\omega_+^* = 5.164$ and $\Delta\hat{\psi}_+ = 0.931$. Based on these parameters, we choose $c = 1.1$. It is important to point out that this value of c may not be suitable for all cases. Further research in this direction is required.

III. Finer Time-Scale Resolution

The WT given by (23) are obtained at $(k/2^j, 1/2^j)$, which is sufficient in the sense that all the information about the function is contained in these coefficients. In other words the function can be reconstructed from these coefficients. A typical time-scale grid obtained from (23) is shown in Fig. 4. In Fig. 4, we have plotted $1/a$ instead of a, but we will, for convenience, call it time-scale plot. The function for which the time-scale grid is shown has support as [0, 1] and has been discretized with step size 2^{-7}, hence mapped into V_7. It is worth pointing out here that there will be a few coefficients outside [0, 1] also because of the finite support of the wavelet.

It is obvious from Fig. 4 that for visual display of the IWT, which is very important for better observation of the function behavior over the time-scale plane, one needs to compute the

IWT on a dense set. In this section we give an outline of the method to get a continuous plot. The mathematical details of the method are given in [24].

The sequences $\{a_k\}$ and $\{b_k\}$ of (25) for splines and the spline wavelets are infinite, although they decay exponentially [11, pp. 200, 266]. In order to compute IWT efficiently, we would like to use sequences $\{p_k\}$ and $\{q_k\}$, which are, as is clear from (13), finite, and this is equivalent to mapping the original function into the dual spline space.

$$f(t) \mapsto f_\beta(t) = \sum_k c_k \phi(\beta t - k) = \sum_k \check{c}_k \tilde{\phi}(\beta t - k). \tag{29}$$

where $\check{c}_k$ and c_k are related as [24]

$$\check{c}_k = \sum_\ell c_\ell \langle \phi(t-\ell), \phi(t-k) \rangle. \tag{30}$$

and ℓ assumes finite values. (See [24] and [27].)

For linear and cubic splines, the relationship is given below:

$\underline{m=2}$

$$\check{c}_l = \frac{1}{3!}(c_{l-1} + 4c_l + c_{l+1}), \tag{31}$$

$\underline{m=4}$

$$\check{c}_l = \frac{1}{7!}(c_{l-3} + 120c_{l-2} + 1191c_{l-1} + 2416c_l + 1191c_{l+1} + 120c_{l+2} + c_{l+3}). \tag{32}$$

Having mapped the function into dual spline space, we can replace $(\{a_k\}, \{b_k\})$ by $(\{(1/2)p_{-k}\}, \{(1/2)q_{-k}\})$ [11, p. 156]. So for real-valued functions, computation of WC at every point (u, v) in the time-scale plane requires 5 multiplications and 4 additions in case of linear spline and 11 multiplications and 10 additions in case of cubic spline. To get the coefficient for an approximate function at that point, the corresponding requirements are 3 and 2 for linear spline and 5 and 4 for cubic spline. For a FFT-based computation scheme, this is not the case since both the function and the wavelet have to be sampled with the same rate and the sampling rate is determined by the highest frequency content of the function. The sampling rate must be kept the same for each subsequent scales in order to keep the function discretization fixed. As a result, the complexity increases with increasing values of the scale parameter a. Furthermore, even at the highest frequency where the support of the wavelet is shortest in time, the number of sampled data for wavelet will be significantly higher than number of q_k.

The time-resolution is bounded from above by the initial level of approximation. In other words, if a function is initially mapped into V_M, then the highest time resolution is $1/2^M$, which can be maintained for each level $j < M$ [24]–[26]. Observe that the time resolution given at level j by standard method is $1/2^j$. The Algorithm (25) is modified to yield the highest time-resolution. Details of the modified decomposition algorithm can be found in [24] and [25].

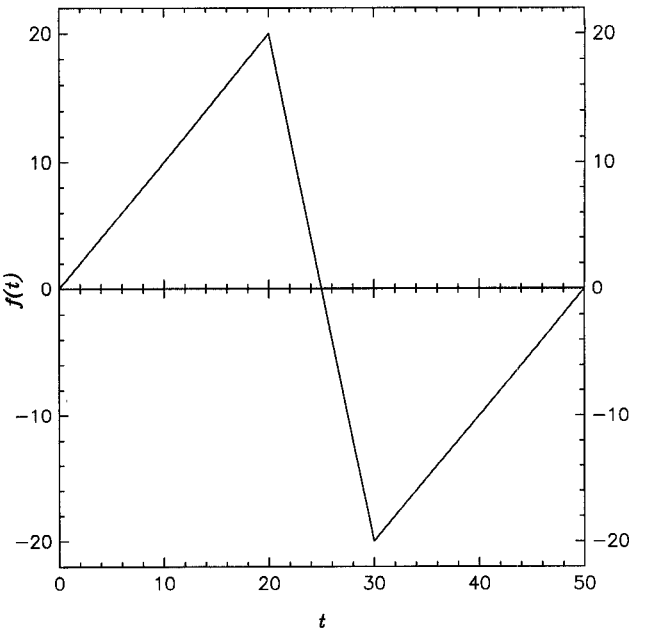

Fig. 5. Linear function whose WT is shown in Figs. 6–8.

The results presented in the next section are for linear and cubic splines. The method can be extended to any splines of higher orders. For cubic spline, we use the local optimal order spline interpolation to map the given data into appropriate spline space, namely

$$f(t) \mapsto f_M(t) = \sum_k c_k^M N_4(2^M t - k), \tag{33}$$

where

$$c_k^M = \sum_{n=k-2}^{k+6} v_{k+2-2n} f\left(\frac{n}{2^{M-1}}\right).$$

Coefficients $\{v_k\}$ are given in [11, p. 117]. The above interpolation formula is "local" and reproduces all the polynomials of at most degree 3.

Unlike the case of linear splines where a function given at integer points is mapped into V_0, in the case of cubic splines for the same data set, the function is mapped into V_1. Hence, for a given set of function values, IWT with cubic spline-wavelet as the analyzing wavelet, gives time-resolution that is of one level higher than the one obtained with linear splines.

For finer scale resolution, we use scaling functions and wavelets that are stretched in time and which, therefore, cover narrower frequency bands.

Let us define the new scaling function and the corresponding wavelet as

$$\phi^n(t) := (\alpha_{n,N})^{1/2} \phi(\alpha_{n,N} t)$$
$$\psi^n(t) := (\alpha_{n,N})^{1/2} \psi(\alpha_{n,N} t), \tag{34}$$

where

$$\alpha_{n,N} = \frac{2^N}{n + 2^N}, N > 0 \quad \text{and} \quad n = 1, \cdots, 2^N - 1. \tag{35}$$

Observe that $1/2 < \alpha_{n,N} < 1$. Applying (34), we get $2^N - 1$ additional levels between two consecutive octaves $[j, j+1]$.

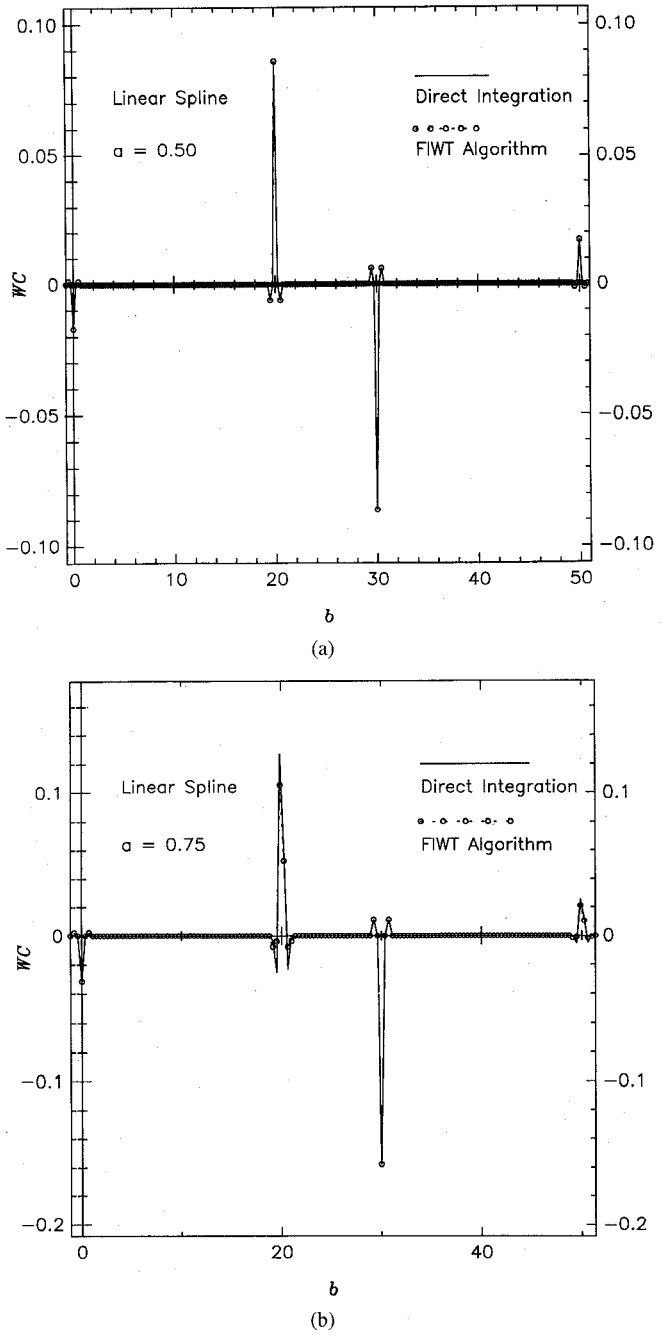

Fig. 6. (a) WT of the function shown in Fig. 5 using linear spline wavelet for $a = 0.50$. Direct integration is performed with $f_2(t)$, the approximation of the function of Fig. 5 at the level $j = 2$. (b) WT of the function shown in Fig. 5 using linear spline wavelet for $a = 0.75$. Direct integration is performed with $f_2(t)$, the approximation of the function of Fig. 5 at the level $j = 2$.

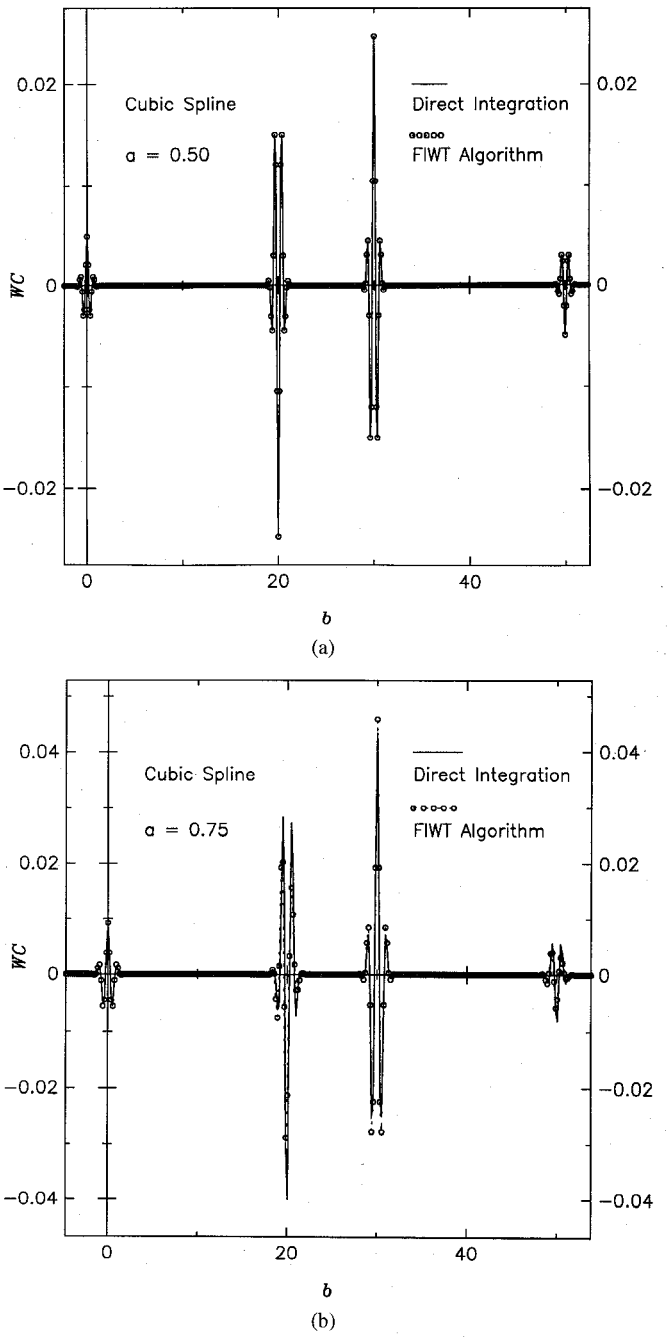

Fig. 7. (a) WT of the function shown in Fig. 5 using cubic spline wavelet for $a = 0.50$. Direct integration is performed with $f_3(t)$, the approximation of the function of Fig. 5 at the level $j = 3$. (b) WT of the function shown in Fig. 5 using cubic spline wavelet for $a = 0.75$. Direct integration is performed with $f_3(t)$, the approximation of the function of Fig. 5 at the level $j = 3$.

The initial sequence $\boldsymbol{c}^M$ is mapped to $\boldsymbol{c}^{M,n}$ for each n [24] which implies that the function f_M is mapped into $f_{M,n}$. Then we proceed with the modified decomposition algorithm using $(\{p_k\}, \{q_k\})$.

It is to be pointed out here that unlike the mapping $\boldsymbol{c}^M \mapsto \tilde{\boldsymbol{c}}^M$, the mapping $\boldsymbol{c}^M \mapsto \boldsymbol{c}^{M,n}$ is not exact. However, for practical purposes, the error is negligible provided that M is sufficiently large.

Furthermore, it can be shown that for all inter-octave scales, time resolution is $\frac{1}{2^M \alpha_{n,N}}$, which is slightly worse than $1/2^M$—the time resolution for the octave levels. It is still better than the best resolution available using the standard algorithm, in which case the highest resolution is $1/2^{M-1}$.

IV. Results and Discussions

The results presented in this section are the centered integral wavelet transform (CIWT) defined with respect to spline wavelet ψ_m as

$$(W_{\psi_m} f)(b, a) := a^{-(1/2)} \int_{-\infty}^{\infty} f(t) \overline{\psi_m \left(\frac{t-b}{a} + t^* \right)} \, dt \tag{36}$$

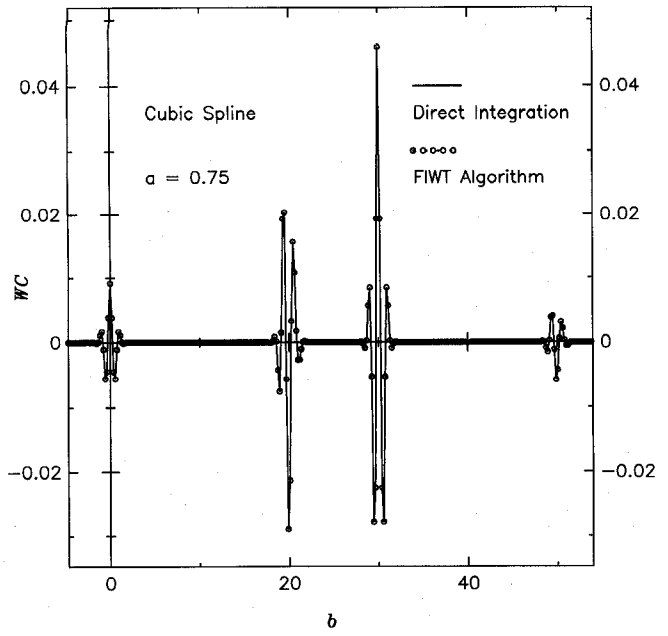

Fig. 8. WT of the function shown in Fig. 5 using cubic spline wavelet for $a = 0.75$. Direct integration is performed with $f_{3,1}(t)$, the approximation of the function of Fig. 5 at the level $j = 3$, $n = N = 1$.

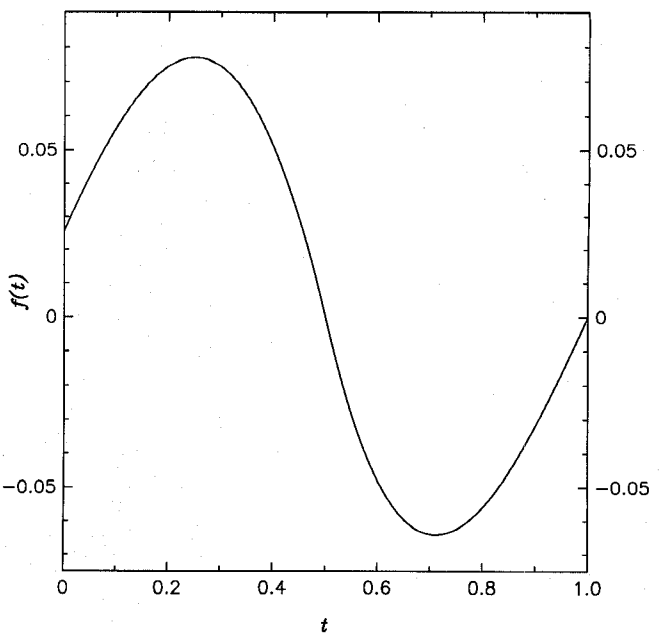

Fig. 9. Graph of the function given by (38).

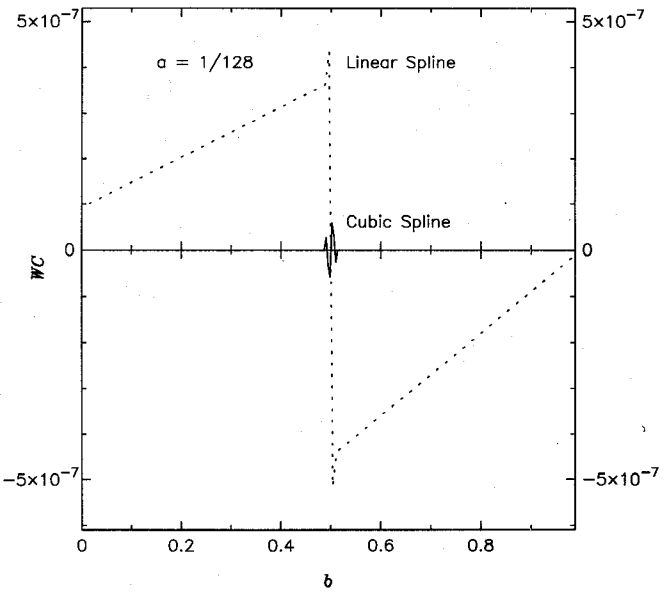

Fig. 10. WT of the function shown in Fig. 9 using linear and cubic spline wavelets for $a = 1/128$. The edge effects are not shown.

where

$$t^* = \frac{2m-1}{2}. \tag{37}$$

Note that in (36) the dual wavelet has not been used since we are using $(\{p_k\}, \{q_k\})$ sequences for decomposition.

The IWT as defined by (17) does not indicate the location of discontinuity of a function properly, since wavelets as shown in Fig. 2 and their duals are not symmetric with respect to zero. The CIWT circumvents this problem by shifting the location of the WC in the time-axis by at^* towards the right.

Example 1: In order to compare the results obtained by the method presented in this paper with the results obtained by evaluating the integral of (36), we first take the linear function that changes slope, as shown in Fig. 5.

The function is sampled with 0.25 as step size. So for linear splines, it means that the function is mapped into V_2, whereas for the cubic splines the function is mapped into V_3. We choose $N = 1$, which gives one additional scale between two consecutive octaves. It is clear from Figs. 6 and 7 that both FIWT algorithm and direct integration give identical results for wavelet coefficients for octave levels, but there are errors in the results for inter-octave levels, as discussed before.

The importance of moment property becomes clear from Figs. 6 and 7. In both the linear and cubic cases, when the wavelet is completely inside the smooth region of the function, the WC are close to zero since the function is linear. Wherever the function changes the slope, WC have larger magnitudes. We also observe the edge-effects near $t = 0$ and $t = 50$. The edge effects can be avoided by using special wavelets near the boundaries [28]. If we use IWT instead of CIWT, then the whole plot will be shifted towards the left and the shift will continue to become larger for lower levels.

For Figs. 6 and 7, the direct evaluation of (36) is done with $f_2(t)$ and $f_3(t)$ respectively. In Fig. 8, the direct integration is done with $f_{3,1}(t)$, which indicates that for inter-octave level also, the FIWT algorithm gives identical results if compared with the corresponding approximation function.

For Fig. 7(a), 440 wavelet coefficients have been computed. The direct integration takes about 300 times more cpu time than the FIWT algorithm. We wish to emphasize that the ratio 300 : 1 is minimum, since with the increase in scale parameter a, the complexity of the direct integration method increases exponentially while for the FIWT it remains almost constant. Furthermore, in the FFT based algorithm, the complexity increases with a.

Example 2: As a further example to highlight the importance of the IWT in identifying the change in function

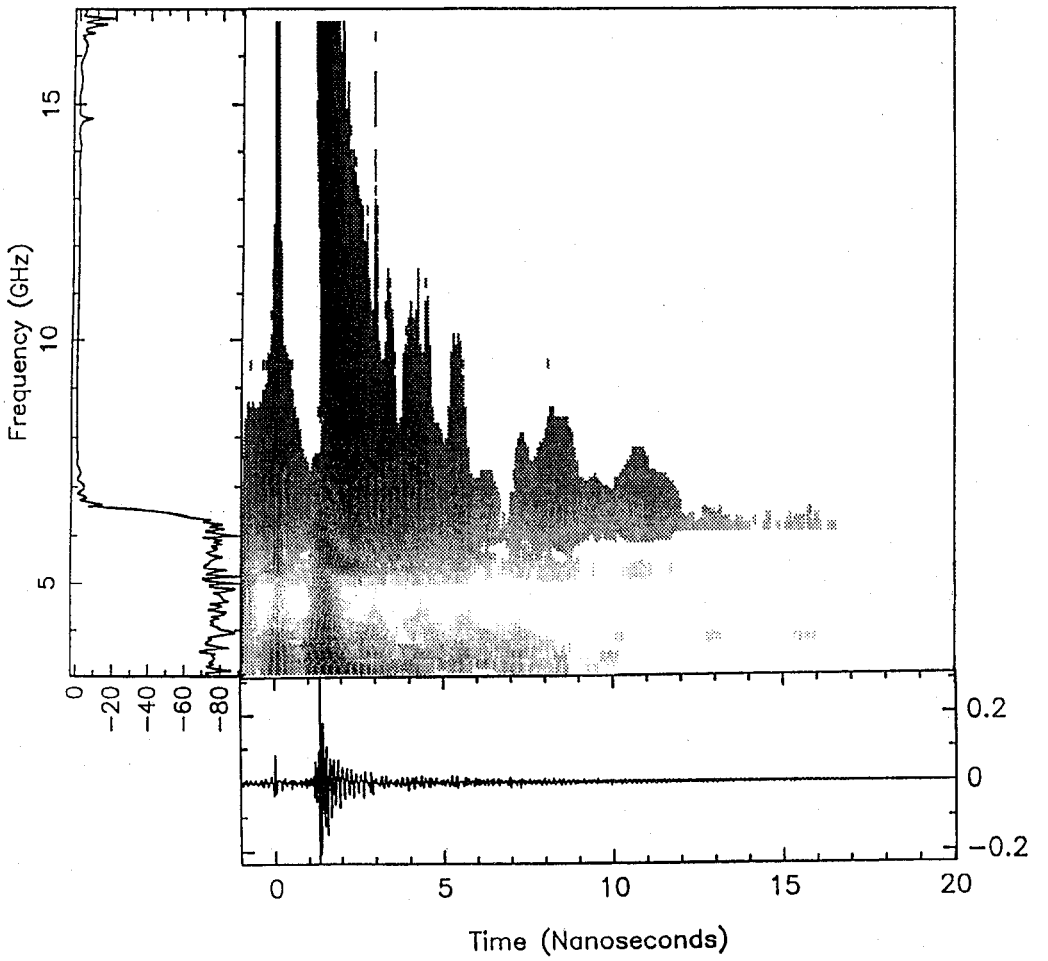

Fig. 11. WT of the experimental data for transmission coefficient of an X-band rectangular waveguide using cubic spline wavelet.

behaviors, we consider the following function (see Fig. 9):

For $y := 2t - 1$

$$f(t) := \begin{cases} -\frac{3}{117}y(4y^2 + 16y + 13) & t \in [0, 1/2] \\ -\frac{1}{6}y(y-1)(y-2) & t \in (1/2, 1]. \end{cases} \quad (38)$$

Fig. 10 shows the WC for linear and cubic splines case. The edge effect has not been shown. Once again, here, we observe that for the cubic spline case, the WC are close to zero in the smooth region of the function, however, for linear spline case, the WC are nonzero in this region since the function is of degree 3 in both intervals. This example shows that even physically unnoticeable discontinuity can be detected using the wavelet transform.

Example 3: As a final example, we find the wavelet transform of experimental data obtained for transmission coefficient of an X-band rectangular waveguide. The waveguide is excited by a coaxial-line probe inserted through the center of the broad side of the waveguide. The S_{21} parameter of the waveguide is measured using 8510 network analyzer by sweeping the input frequency from 2–17 GHz. The time domain waveform is obtained by inverse Fourier transforming the frequency domain data. The time response (upto a constant multiplier) and the magnitude (in dB) of the frequency response are shown in Fig. 11. It should be pointed out here that several low-amplitude impulses appeared in the negative time axis, but they have not been taken into account while performing the wavelet decomposition since they represent some unwanted signals and can be removed from the plot by proper thresholding. Furthermore, such omission will not have any significant effect on the WC plot of Fig. 11 because of the local nature of wavelet analysis.

The cut-off frequency and dispersive nature of the dominant TE_{10} is well observed from its time-frequency plot. Because of the guide dimension and excitation, the next-higher-order degenerate modes are TE_{11} and TM_{11} with cut-off frequency as 16.156 GHz. This does not appear on the plot. The plot indicates some transmission taking place below the lower frequency operation. There is a short pulse at $t = 0$, which contains all the frequency components and is almost nondispersive. These can be attributed to the system noise. No further attempt has been made to isolate the effects of various transitions used in the experiment. The thresholding for Fig. 11 has been done with respect to the relative magnitude (in dB) of the local maximum of each frequency and global maximum. Finally the magnitude of the wavelet coefficients has been mapped to 8-bit gray scale levels.

A better time-frequency localization can be obtained by using higher order spline wavelets. (See [27, ch. 4].)

V. Conclusion

In this paper we have presented a technique for efficient computation of the integral wavelet transform of a finite-

energy function on a dense set of the time-scale (time-frequency) domain by using compactly supported spline-wavelets. Unlike the case with the standard method, which is applicable for binary scales only, our method can be used for arbitrary scale parameters. A number of examples have been included to highlight the important properties of the integral wavelet transform. Finally, the experimental data obtained for waveguide transmission have been analyzed, indicating the dispersive nature of the mode propagation.

ACKNOWLEDGMENT

The authors would like to acknowledge the assistance of Mr. S. Kanamaluru of the Electromagnetics and Microwave Laboratory in obtaining the experimental data. J. C. Goswami would like to thank the IEEE MTT Society for providing him with the Graduate Student Fellowship in 1993 and 1994.

REFERENCES

[1] G. Beylkin, R. Coifman, and V. Rokhlin, "Fast wavelet transform and numerical algorithms I," *Comm. Pure Appl. Math.*, vol. 44, pp. 141–183, 1991.

[2] B. K. Alpert, "Wavelets and other bases for fast numerical linear algebra," in *Wavelets: A Tutorial in Theory and Applications*, C. K. Chui, Ed. Boston: Academic, 1992, pp. 181–216.

[3] S. Jaffard and P. Laurençot, "Orthonormal wavelets, analysis of operators, and applications to numerical analysis," in *Wavelets: A Tutorial in Theory and Applications*, C. K. Chui, Ed. Boston: Academic, 1992, pp. 655–678.

[4] B. K. Alpert, "A class of bases in L^2 for the sparse representation of integral operators," *SIAM J. Math. Anal.*, vol. 24, pp. 246–262, Jan. 1993.

[5] B. K. Alpert, G. Beylkin, R. Coifman, and V. Rokhlin, "Wavelet-like bases for the fast solution of second-kind integral equations," *SIAM J. Sci. Comp.*, vol. 14, pp. 159–184, Jan. 1993.

[6] R. Glowinski, W. Lawton, and M. Ravachol, "Wavelet solutions of linear and nonlinear elliptic, parabolic and hyperbolic problems in one space dimension," in *Computing Methods in Applied Sciences and Engineering*, R. Glowinski and A. Lichnewsky, Eds. Philadelphia: SIAM, 1990, pp. 55–120.

[7] J. C. Xu and W. C. Shann, "Galerkin-wavelet methods for two-point boundary value problems," *Num. Math.*, vol. 63, pp. 123–144, 1992.

[8] C. K. Chui and E. Quak, "Wavelets on a bounded intervals," *Num. Math. Approx. Theory.*. D. Braess and L. L. Schumaker, Eds. Basel: Birkhäuser Verlag, vol. 9, 1992, pp. 53–75.

[9] P. Auscher, "Wavelets with boundary conditions on the interval," in *Wavelets: A Tutorial in Theory and Applications*, C. K. Chui, Ed. Boston: Academic, 1992, pp. 217–236.

[10] V. Perrier, "Towards a method for solving partial differential equations using wavelet bases," in *Wavelets, Time-Frequency Methods and Phase Space*, J. M. Combes, A. Grossmann, and P. Tchamitchian, Eds. Berlin: Springer-Verlag, 1989, pp. 269–283.

[11] C. K. Chui, *An Introduction to Wavelet*. Boston: Academic, 1992.

[12] I. Daubechies, *Ten Lectures on Wavelets, CBMS-NSF series in Applied Maths No. 61*. Philadelphia: SIAM, 1992.

[13] H. Kim and H. Ling, "Wavelet analysis of radar echo from finite-size target," *IEEE Trans. Antennas Propagat.*, pp. 200–207, Feb. 1993.

[14] G. Kaiser, "Wavelet electrodynamics," *Phys. Lett. A.*, vol. 168, pp. 28–34, 1992.

[15] L. C. Kempel, "Wavelets and electromagnetics," Michigan Radiation Lab. Rep., Dec. 1991.

[16] B. Z. Steinberg and Y. Leviatan, "On the use of wavelet expansions in method of moments," *IEEE Trans. Antennas Propagat.*, pp. 610–619, May 1993.

[17] R. L. Wagner, P. Otto, and W. C. Chew, "Fast waveguide mode computation using wavelet-like basis functions," *IEEE Microwave and Guided Wave Lett.*, vol. 3, pp. 208–210, July 1993.

[18] A. Moghaddar and E. K. Walton, "Time-frequency distribution analysis of scattering from waveguide cavities," *IEEE Trans. Antennas Propagat.*, pp. 677–680, May 1993.

[19] C. K. Chui and J. Z. Wang, "On compactly supported spline wavelets and a duality principle," *Trans. Amer. Math. Soc.*, vol. 330, pp. 903–915, 1992.

[20] K. Kalbasi and K. R. Demarest, "A multilevel formulation of method of moments," *IEEE Trans. Antennas Propagat.*, pp. 589–599, May 1993.

[21] Y. Meyer, *Ondelettes et Opérateurs*. Paris: Hermann, 1990.

[22] S. G. Mallat, "Multiresolution approximations and wavelet orthonormal bases of $L^2(\mathbb{R})$," *Trans. Amer. Math. Soc.*, vol. 315, pp. 69–87, 1989.

[23] C. K. Chui, *Multivariate Splines, CBMS-NSF series in Applied Maths No. 54*. Philadelphia: SIAM, 1988.

[24] C. K. Chui, J. C. Goswami, and A. K. Chan, "Fast integral wavelet transform on a dense set of time-scale domain," to be published in *Numer. Math.*

[25] M. J. Shensa, "The discrete wavelet transform: Wedding the À trous and Mallat algorithms," *IEEE Trans. Signal Processing*, vol. 40, pp. 2464–2482, Oct. 1992.

[26] O. Rioul and P. Duhamel, "Fast algorithms for discrete and continuous wavelet transforms ," *IEEE Trans. Inform. Theory*, vol. 38, pp. 569–586, Mar. 1992.

[27] C. K. Chui, *Wavelets: For Time-Frequency Analysis*. Philadelphia: SIAM, to be published.

[28] E. Quak and N. Weyrich, "Decomposition and reconstruction algorithms for spline wavelets on a bounded interval," *Appl. and Computational Harmonic Analysis*, vol. 1, no. 3, pp. 217–231, June 1994.

Jaideva C. Goswami (S'86–A'87–S'88–M'90–S'92) was born in 1964 in Khutauna, Bihar state, India. He received the B.E. degree (electronics) from Regional Engineering College, Surat in 1986 and M.Tech. degree (electrical) from Indian Institute of Technology, Kanpur in 1989.

He was on the faculty of Regional Engineering College, Surat in 1987. Prior to joining Texas A&M University in 1991 as a Ph.D. student, he worked at the Advanced Center for Electronic Systems, Indian Institute of Technology, Kanpur, as a research engineer for two years. His research interests include application of wavelets in computational electromagnetics, time-frequency signal analysis, inverse problems, and nonlinear optics.

Mr. Goswami won the IEEE-MTT Graduate Student Fellowship Award in 1993 and 1994.

Andrew K. Chan (S'63–M'77–SM'89) received the Ph.D. degree in electrical engineering in 1971 from the University of Washington at Seattle.

He is currently professor of the Department of Electrical Engineering at Texas A&M University. His research interests include propagation of electromagnetic and acoustic waves, high power semiconductor laser design, nonlinear wave propagation in guiding structures, numerical approximation theory, and wavelet signal processing.

Charles K. Chui (S'79–M'90–F'94), Distinguished Professor of Mathematics and Professor of Electrical Engineering and of Statistics at Texas A&M University, is the Director of the Center for Approximation Theory and the Wavelet Research Laboratory. He received the Ph.D. degree from the University of Wisconsin, Madison, in 1967.

He has held visiting positions in various universities in the past, including Florence and Bologna (Italy, 1979 and 1992), Canterbury (New Zealand, 1987), and Cambridge (England, 1987). His current research interests are mathematical analysis, wavelets, and signal processing. Serving on the editorial board of nine journals in mathematics and electrical engineering, he is co-Editor-in-Chief of the interdisciplinary journal, *Applied and Computational Harmonic Analysis* (ACHA): time-frequency, time-scale analysis, wavelets, numerical algorithms, and applications, published by Academic. Dr. Chui has published over 230 papers and 17 books, including three volumes in the *Springer Series in Information Sciences*, published by Springer Verlag, as well as the volume *An Introduction to Wavelets*, published by Academic. Currently, he is also the editor of two book series: *Wavelet Analysis and Its Applications*, published by Academic; and *Approximations and Decompositions*, published by World Scientific.

Dr. Chui is a member of AMS, MAA, and SIAM.